



**1 Comprehensive evaluation of typical planetary boundary
2 layer (PBL) parameterization schemes in China. Part II:
3 Influence of uncertainty factors**

4 Wenxing Jia¹, Xiaoye Zhang^{1,2*}, Hong Wang¹, Yaqiang Wang¹, Deying Wang¹, Junting Zhong¹,
5 Wenjie Zhang¹, Lei Zhang¹, Lifeng Guo¹, Yadong Lei¹, Jizhi Wang¹, Yuanqin Yang¹, Yi Lin³

6 ¹State Key Laboratory of Severe Weather & Key Laboratory of Atmospheric Chemistry of CMA,
7 Chinese Academy of Meteorological Sciences, Beijing, 100081, China

8 ²Center for Excellence in Regional Atmospheric Environment, IUE, Chinese Academy of Sciences,
9 Xiamen, 361021, China

10 ³Key Laboratory for Mesoscale Severe Weather, Ministry of Education, and School of Atmospheric
11 Sciences, Nanjing University, Nanjing, China

12 Correspondence to: X. Zhang (xiaoye@cma.gov.cn)

13
14
15
16
17
18
19
20
21
22
23
24
25
26
27
28
29
30



31 Abstract. This study focuses on the uncertainties that influence numerical simulation results of
32 meteorological fields (including horizontal resolution, vertical resolution, near-surface scheme,
33 initial and boundary conditions, underlying surface update, and update of model version). By further
34 evaluating and analyzing the uncertainty factors, it is expected to provide relevance for those
35 scholars who are devoted to factor analysis, in order to make the results closer to the observed values.
36 In this study, a total of 12 experiments are set up to analyze the effects of the uncertainties mentioned
37 above, and the following conclusions are drawn: (1) Horizontal resolution has a greater effect than
38 vertical resolution. (2) The simulated effects of temperature and wind speed in the near-surface
39 scheme are smaller than those in the PBL scheme. (3) The initial and boundary conditions of
40 different products have the most remarkable effect on relative humidity, and the simulation results
41 of EC data are the best. (4) The updates with urban and water bodies as the underlying surface have
42 a more significant contribution to the meteorological fields, especially on temperature. (5) The
43 update of the model version does not necessarily optimize the model results. In general, the
44 configuration of uncertainties needs to be considered comprehensively according to what you need
45 in order to obtain the best simulation results.

46

47 Introduction

48 The key factor for the accurate simulation of near-surface meteorological elements and planetary
49 boundary layer (PBL) structure is the PBL parameterization scheme. Part I has discussed the impact
50 of the PBL scheme in detail from the mechanism, and assessed the applicability of the PBL scheme
51 for different parameters in different regions and seasons. However, there are still many uncertainties
52 in the model that can affect the forecasts and results. The model settings used by different scholars
53 exhibit differences in the simulation results. For example, the horizontal and vertical resolutions are
54 essential for model settings. Horizontal resolution, as a critical factor, must be considered in all
55 models, whether they are macroscale earth system models (ESMs), climate models, mesoscale
56 regional models, or microscale fluid models. Constrained by computational resources, a horizontal
57 resolution of about 100~250 km is used for ESMs models (e.g., Coupled Model Intercomparison
58 Project phase 6, CMIP6 model) (D. Li et al., 2022; Taylor, Stouffer, & Meehl, 2012). The horizontal
59 resolution of climate models typically ranges from 50 to 25 km (e.g., Flexible Global Ocean-
60 Atmosphere-Land System Finite-Volume version 3, FGOALS-f3 model)(J. Li et al., 2021). The



61 horizontal resolution of mesoscale weather models (e.g., The Global/Regional Assimilation
62 Prediction System, GRAPES model, Weather Research and Forecasting, WRF model)(García-
63 García, Cuesta-Valero, Beltrami, González-Rouco, & García-Bustamante, 2022; Ma et al., 2018)
64 can be as fine as 1 km. The microscale fluid models can have a horizontal resolution of less than
65 100 m (e.g., Large eddy simulation, LES model)(Zhou, Zhu, & Xue, 2017). Studies have shown
66 that the interaction between large- and small-scales is influenced by resolution, with finer resolution
67 allowing for better characterization of underlying surface features and extreme
68 events(Rummukainen, 2016; Singh et al., 2021), and also impacting future climate
69 predictions(Chang et al., 2020; Roberts et al., 2020; Small et al., 2014). The use of PBL scheme is
70 usually in coarse resolution models, which can lead to additional errors since these schemes are
71 developed for flat terrain conditions(Weigel, Chow, & Rotach, 2007).

72 Finer vertical resolution can better capture changes in PBL structure, which can also have an impact
73 on mass transport(Menut, Bessagnet, Colette, & Khvorostyanov, 2013; O'Dea et al., 2017; Teixeira,
74 Carvalho, Tuccella, Curci, & Rocha, 2016), especially on the accuracy of wind resources (Tolentino,
75 Rejuso, Inocencio, Ang, & Bagtasa, 2016). In addition, horizontal and vertical resolutions can cause
76 spurious gravity waves and increase model errors(Nolan & Onderlinde, 2022). Although higher
77 resolution is better, there is no doubt that it is computationally expensive. Whether the use of finer
78 resolution will bring significant improvement to the model results deserves further discussion.

79 Different PBL schemes are combined with the different near-surface (N-S) schemes, both of which
80 are crucial to the simulation results of the meteorological fields. For instance, the MYJ scheme (i.e.,
81 PBL scheme) can only couple the Eta scheme (i.e., N-S scheme), while the BL scheme (i.e., PBL
82 scheme) can couple both the MM5 and the Eta schemes (i.e., N-S scheme). The N-S scheme is
83 pivotal for mesoscale numerical simulation, especially for fine numerical forecasting(Y. Li, Gao,
84 Lenschow, & Chen, 2010). Then, to figure out which scheme has a greater impact on the
85 meteorological field will help to make targeted improvements to the forecasts in the future. In
86 addition, the lag of the underlying surface data can also affect the simulation results of the
87 meteorological fields, especially for large cities with relatively rapid urbanization (Qian et al., 2022).

88 The European Center for Medium-Range Weather Forecasting (ECMWF, hereafter referred to as
89 EC) has concluded that the steady progress in numerical forecasting over the last 30 years is mainly
90 attributed to improvements in the forecast models themselves, the application of more observations
91 and the development of data assimilation techniques(Magnusson & Källén, 2013). Among them,



92 the performance of the forecast model depends largely on the model resolution, the accuracy of the
93 finite difference method, and the representativeness of the physical process parameterization
94 scheme. Different initial fields also influence the model results due to different observational data,
95 quality control methods, assimilation schemes, and bias correction methods adopted for different
96 reanalysis data(Ma et al., 2021).
97 Finally, we also have to take the update of the model version into account. With model versions
98 being updated, many parameterization schemes are more or less updated(Morichetti et al., 2022).
99 However, under the circumstance that the updates are not disclosed in scientific and technical reports
100 or papers, we need to dig into them from the code itself. In reality, simulation results will be likely
101 to vary from scholar to scholar because of different model versions they choose. Consequently, it is
102 necessary to adopt a control variable approach when discussing the impact of model version updates.
103 Instead of updating all parameterization schemes, only by updating the ones we are concerned with
104 can the uncertainty arising from version updates can be quantified.
105 These aforementioned uncertainties have been studied by scholars individually, but few scholars
106 have been able to synthesize and analyze these factors. In this part, each of these uncertainties will
107 be analyzed and discussed, and the factors with more significant effects will be selected for reference
108 in that identifying which factors besides the PBL scheme are critical to the simulation of
109 meteorological fields makes all the difference.

110

111 2. Data and Methodology

112 2.1 Data

113 2.1.1 Reanalysis Data

114 *Final (FNL) reanalysis data.* The National Centers for Environmental Prediction (NCEP)
115 global final (FNL) reanalysis data are based on the 6 h temporal resolution (i.e., 00:00 (08:00),
116 06:00 (14:00), 12:00 (18:00), 18:00 (02:00) UTC (BJT)) by the Global Data Assimilation
117 System (GDAS) with a resolution of $1^\circ \times 1^\circ$ or $0.25^\circ \times 0.25^\circ$. This product continuously
118 collects observational data from the Global Telecommunications System (GTS) and other
119 sources. The FNL reanalysis data are made with the same model as NCEP uses in the Global
120 Forecast System (GFS), but the FNL reanalysis data are prepared about an hour or so after the



121 GFS is initialized. The FNL reanalysis data parameters include surface pressure, sea level
122 pressure, geopotential height, temperature, sea surface temperature, soil values, ice cover,
123 relative humidity, winds, vorticity etc. The data temporal range for 1-degree is from July 30,
124 1999 to the present, while the time range for the 0.25-degree is from July 8, 2015 to the present
125 (<https://rda.ucar.edu/datasets/ds083.2/>, <https://rda.ucar.edu/datasets/ds083.3/>).

126 *The fifth generation ECMWF reanalysis (ERA5) data.* The ERA5 is the fifth generation
127 ECMWF reanalysis of the global climate. Reanalysis combines model data with observations
128 worldwide to form a globally complete and consistent dataset. ERA5 replaces its predecessor,
129 the ERA-Interim reanalysis. ERA5 data is available from 1959 to present with a resolution of
130 $0.25^\circ \times 0.25^\circ$ (atmosphere) and $0.5^\circ \times 0.5^\circ$ (ocean waves). The model requires 3D data and
131 2D DATA, and the variables of 3D data are temperature, U and V components of wind,
132 geopotential height, relative humidity
133 ([https://cds.climate.copernicus.eu/cdsapp#!/dataset/reanalysis-era5-pressure-](https://cds.climate.copernicus.eu/cdsapp#!/dataset/reanalysis-era5-pressure-levels?tab=overview)
134 [levels?tab=overview](https://cds.climate.copernicus.eu/cdsapp#!/dataset/reanalysis-era5-pressure-levels?tab=overview)). The 2D data mainly includes the parameters surface pressure, mean sea
135 level pressure, skin temperature, 2-m temperature, 2-m relative humidity, 10-m U and V
136 components of wind, soil data and soil height
137 ([https://cds.climate.copernicus.eu/cdsapp#!/dataset/reanalysis-era5-single-](https://cds.climate.copernicus.eu/cdsapp#!/dataset/reanalysis-era5-single-levels?tab=overview)
138 [levels?tab=overview](https://cds.climate.copernicus.eu/cdsapp#!/dataset/reanalysis-era5-single-levels?tab=overview)).

139 2.1.2 Underlying surface data

140 The default underlying surface data in WRF are USGS and MODIS data, where USGS has 24
141 classifications and MODIS has 20 classifications. In this study, MODIS data is selected. The
142 basic land cover is a modified IGBP (International Geosphere Biosphere Programmer), which
143 is calculated by supervised classification using MODIS Terra and Aqua reflectance data, with
144 a resolution of 500 m
145 (https://www2.mmm.ucar.edu/wrf/users/download/get_sources_wps_geog.html). The dataset
146 that comes with WRF is based on the year 2001 (Bhati & Mohan, 2016). The 20 types are
147 evergreen needleleaf, evergreen broadleaf, deciduous needleleaf, deciduous broadleaf, mixed
148 forest, closed shrublands, open shrublands, woody savannas, savannas, grasslands, permanent
149 wetlands, croplands, urban and built-up, cropland mosaics, snow and ice, bare soil and rocks,
150 water bodies, wooded tundra, mixed tundra and barren tundra.



151 To consider the influence of the underlying surface data on the model results, we further select
152 the same underlying surface data as the simulation period (i.e., January 2016)
153 (<https://e4ftl01.cr.usgs.gov/MOTA/MCD12Q1.006/>). This data is MCD12Q1 version 6 data
154 product(Friedl et al., 2002), including 17 land types that cover the IGBP land cover
155 classification.

156 **2.2 Description of the modelling experiments**

157 To evaluate the effect of these uncertainties on the simulation results of the meteorological fields, a
158 total of 12 experiments are conducted, and the detailed configuration of the experiments is shown
159 in Table 1. The effect of horizontal resolution is presented by three experimental comparisons in
160 Exp1, Exp2 and Exp3, and the effect of vertical resolution by Exp3 and Exp4. The implications of
161 the surface layer schemes are analyzed by comparing three experiments in Exp5, Exp6 and Exp7.
162 The impact of the initial field and boundary conditions are compared by three experiments, i.e.,
163 Exp3, Exp8 and Exp9. The influences of the underlying surface are displayed by two Exp3 and
164 Exp10. The update of the model version is compared by Exp11 and Exp12.

165 Table 1 detail parameters setting of the experiments

| Experiments | Horizontal resolution | Vertical resolution | PBL schemes | Surface layer schemes | Initial field and boundary condition | Underlying surface | Version of Model |
|-------------|-----------------------|---------------------|-------------|-----------------------|--------------------------------------|--------------------|------------------|
| Exp1 | 75 km | 48 levels | YSU | MM5 | FNL-1 ° | Modis-15s | WRF v3.9.1 |
| Exp2 | 15 km | 48 levels | YSU | MM5 | FNL-1 ° | Modis-15s | WRF v3.9.1 |
| Exp3 | 3 km | 48 levels | YSU | MM5 | FNL-1 ° | Modis-15s | WRF v3.9.1 |
| Exp4 | 3 km | 62 levels | YSU | MM5 | FNL-1 ° | Modis-15s | WRF v3.9.1 |



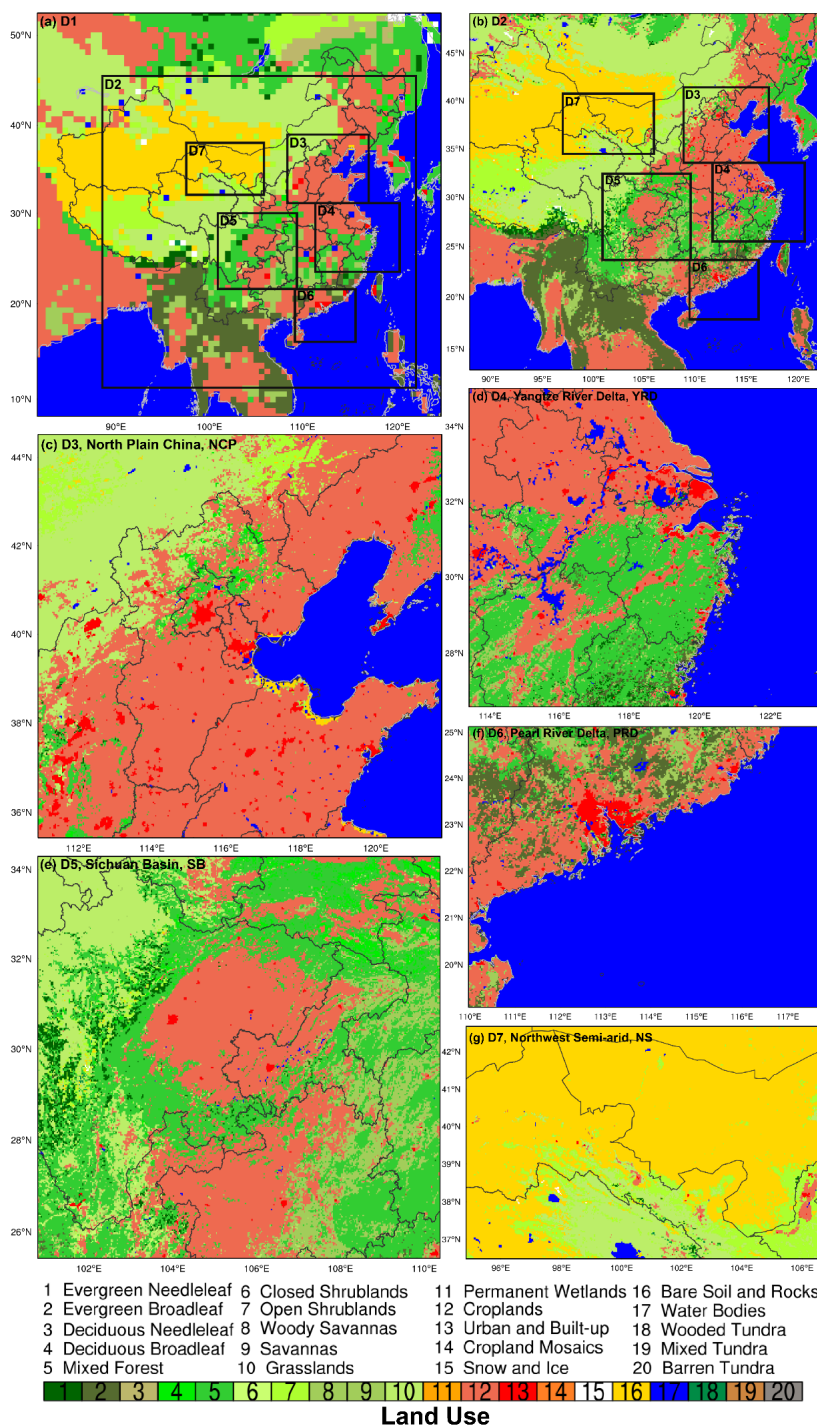
| | | | | | | | |
|-------|------|-----------|------------|------------|------------------------|-----------------------------|-----------------------------------|
| Exp5 | 3 km | 48 levels | BL | MM5 | FNL-1 ° | Modis-15s | WRF v3.9.1 |
| Exp6 | 3 km | 48 levels | MYJ | Eta | FNL-1 ° | Modis-15s | WRF v3.9.1 |
| Exp7 | 3 km | 48 levels | BL | Eta | FNL-1 ° | Modis-15s | WRF v3.9.1 |
| Exp8 | 3 km | 48 levels | YSU | MM5 | FNL- 0.25 ° | Modis-15s | WRF v3.9.1 |
| Exp9 | 3 km | 48 levels | YSU | MM5 | EC-0.25 ° | Modis-15s | WRF v3.9.1 |
| Exp10 | 3 km | 48 levels | YSU | MM5 | FNL-1 ° | Modis-15s (2017) | WRF v3.9.1 |
| Exp11 | 3 km | 48 levels | ACM2 | MM5 | FNL-1 ° | Modis-15s | WRF v3.9.1 |
| Exp12 | 3 km | 48 levels | ACM2 | MM5 | FNL-1 ° | Modis-15s | WRF v3.6.1⁺ |

166 *WRF3.6.1⁺ refers to the migration of the ACM2 scheme from WRFv3.6.1 to WRFv3.9.1, ensuring
167 that no changes in other parameterization schemes.

168 3 Results and discussion

169 3.1 horizontal resolution impact on 2-m temperature and 10-m wind speed

170 The underlying surface information is crucial to the simulation of near-surface meteorological
171 factors. From the distribution of the underlying surface, the three different resolutions of the model
172 can basically capture the general information of the underlying surface (Fig. 1). The resolution of
173 75 km is relatively coarse, so many fine features are ignored and represented uniformly by a large
174 grid (Fig. 1a). The resolution of 15 km is very significantly different compared to 75 km (Fig. 1b),
175 and many fine characteristics (e.g., lakes, cities, etc.) are represented, very close to the features of 3
176 km.



177

178

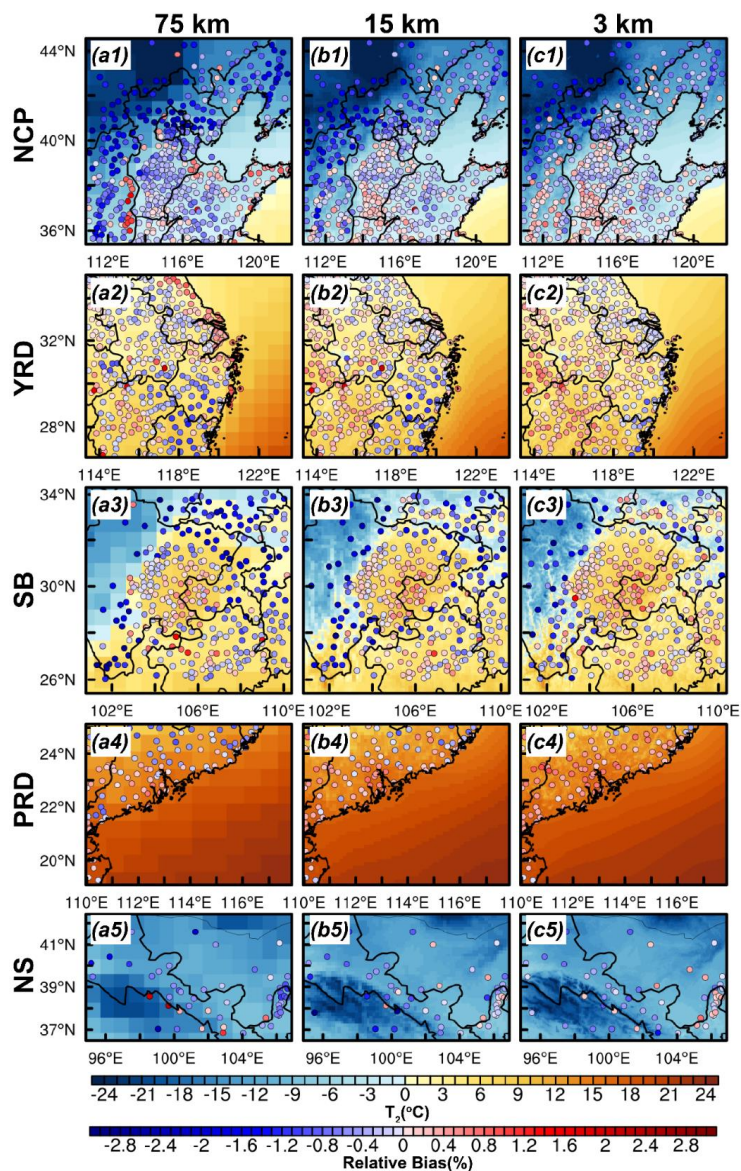
Figure 1. (a-g) Map of land use type in the seven nested model domains.



179 Further comparative analysis of temperature and wind speed in five regions at these three resolutions
180 have been performed. In terms of regional distribution, all three experiments can simulate high and
181 low value areas of 2-m temperature, but there are differences in the degree of overestimation and
182 underestimation (Fig. 2). In the NCP region, the three experiments underestimate the temperature
183 over a similar range of regions, especially in the northwest (Fig. 2a1-c1). Experiment 1 differs more
184 sharply from the other two experiments in areas with more marked underlying surface variability
185 such as in the complex mountainous areas in the northwest, the underestimation of Exp1 is more
186 significant, and at the sea-land interface, the overestimation of Exp1 is more pronounced (Fig. 2a1),
187 because the grid resolution is too low. The number of stations overestimated by the three
188 experiments is 96, 128, 172, and the relative bias are 0.38%, 0.19%, 0.18%. Although the number
189 of stations overestimated by Exp1 is small, there are more extreme values, so the deviation is larger.
190 Correspondingly, the higher degree of underestimation (-0.89%) in Exp1 derives from more
191 minimal values and stations (N=397) as well. For the YRD region, obviously, Fig. 2a2-c2 note that
192 the RB of the stations vary greatly with different horizontal resolutions, especially for the
193 northeastern coastal of YRD region (i.e., northeast Jiangsu province) from overestimation (Fig. 2a2)
194 to underestimation (Fig. 2c2), and the degree of underestimation gradually decreases in the southeast
195 of YRD (i.e., Zhejiang and Fujian provinces). In the SB region, it is clear that Exp1 underestimates
196 the 2-m temperature more significantly (RB=-1.11%, N=245), with fewer stations in the Fig. 2a3,
197 followed by Exp2 (RB=-1.03%, N=208), and to a lesser extent by Exp3 (RB=-0.69%, N=152). The
198 PRD region behaves differently from other regions, with the simulation results of Exp1 showing an
199 underestimation (RB=-0.11%), while Exp2 (RB=0.13%) and Exp3 (RB=0.35%) an overestimation
200 (Fig. 2a4-c4). The variation of underlying surface between grids in the PRD region is more complex
201 in comparison with other regions (Fig. 1). This does not indicate that the simulation results are better
202 when the grid horizontal resolution is lower, because the scheme itself still has errors in the
203 simulation. It only reveals that the simulation results of Exp1 perform better statistically in the
204 current model configuration for this region. The number of stations in Exp1 in the NS region is
205 much less than the other two experiments, which means that the relative bias of Exp1 is more than
206 $\pm 3\%$ and the deviation is greater, for the area along the Qilian mountains (Fig. 2a5-c5) in particular.
207 The results of wind speed are different from those of temperature, and the difference between the
208 three experiments is not as obvious as that of temperature (Fig. 3). The three experiments
209 overestimate the wind speed to varying degrees, however, more stations underestimate wind speed



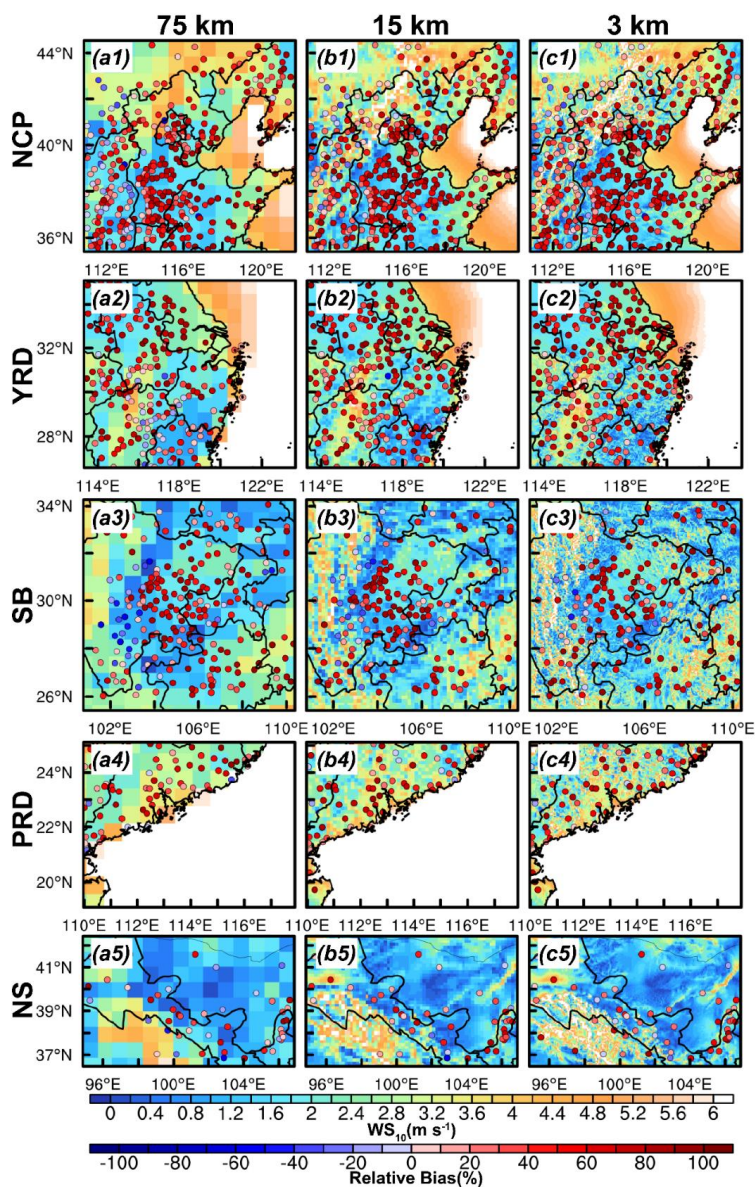
210 in the Exp1, especially in the NCP ($N_{Exp1}=34$, $N_{Exp2}=21$, $N_{Exp3}=19$) and SB region ($N_{Exp1}=29$,
 211 $N_{Exp2}=18$, $N_{Exp3}=7$) (Fig. 3a3). As the grid resolution is too coarse in the Exp1, the wind speed is
 212 underestimated at some stations due to the complex terrain in the NCP and SB regions (Fig. 3a1,
 213 a3).



214
 215 **Figure 2.** Regional distribution of 2-m temperature simulated by the (a) domain 1 (75 km), (b)
 216 domain 2 (15 km) and (c) domain 3 (3 km) for five regions in January, and distribution of relative
 217 bias between simulations and observations is denoted by scatters.



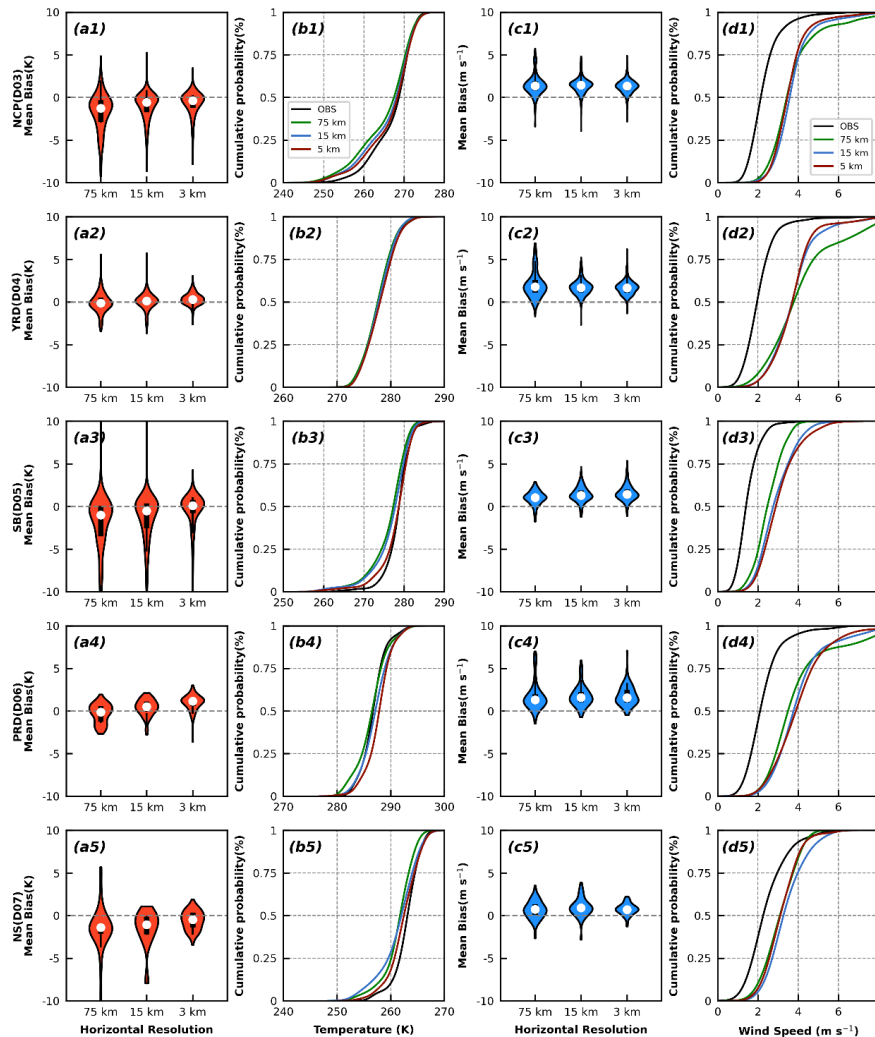
218 It can also be seen from Figure 4 that the three experiments have a large difference in temperature
219 simulation, and the underestimate in Exp1 is more significant (Fig. 4a1-a5). However, in the PRD
220 region, although the average value of the mean bias is closer to 0 on account of the offsetting positive
221 and negative deviations. For the distribution range of the mean bias, it has been found that the
222 distribution of the Exp3 is closer to 0 (Fig. 4a4). In terms of the cumulative probability distribution,
223 the simulations differ for different temperature segments in the NCP, SB, and NS regions. For the
224 NCP region, the temperature below 270 K is better simulated in Exp3, the temperature threshold in
225 the SB region is about 280 K, and the threshold is about 265 K in the NS region (Fig. 4b1, b3, b5).
226 In the YRD region, the simulations of all three experiments are almost the same for any segmented
227 temperature (Fig. 4b2). In addition, the PRD region is special, with temperature below about 285 K,
228 and the Exp2 simulates better (Fig. 4b4). It is worth noting that, regardless of the region, one thing
229 in common is that the temperature of the three experiments simulations gets closer and closer as the
230 temperature increases. While the difference of wind speed between the three experiments is not
231 obvious (Fig. 4c1-c5). The average value of the mean bias in Exp1 is closer to 0, mainly attributable
232 to that there are more stations with negative mean bias to offset. Wind speed and temperature behave
233 differently in regard of cumulative probability distributions, with increasing differences in simulated
234 wind speeds for the three experiments as wind speed increases (Fig. 4d1-d5). The wind speed
235 simulated in Exp1 is low, leading to a better performance in Exp1 for small wind speed (Fig. 4d1-
236 d5).



237

238

Figure 3. Similar as Figure 2, but for 10-m wind speed.



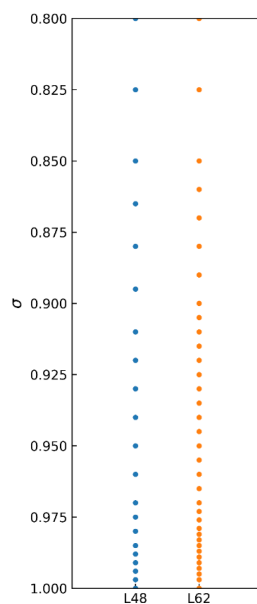
239
 240 **Figure 4.** Violin-plots of mean bias of observed and simulated (a1-a5) 2-m temperature and (c1-c5)
 241 10-m wind speed at different horizontal resolution (i.e., 75 km, 15 km, 3 km), cumulative
 242 probability of observed and simulated (b1-b5) 2-m temperature and (d1-d5) 10-m wind speed at
 243 different horizontal resolution (i.e., 75 km, 15 km, 3 km) for five regions.

244 **3.2 vertical resolution impact on PBL structures**

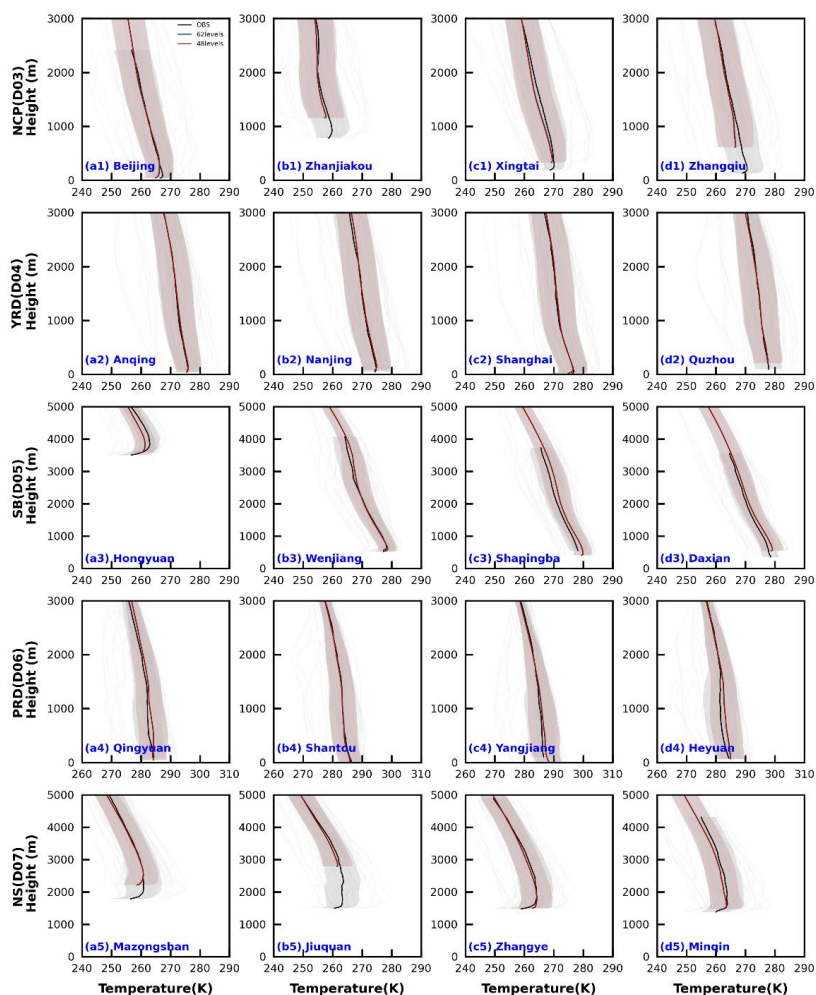
245 Based on Exp3, the vertical resolution has been further encrypted from 21 to 35 levels below 2 km,
 246 i.e., the total number of vertical levels is increased from 48 to 62 levels (Fig. 5). The temperature
 247 and wind fields of the two experiments (Exp3 and Exp4) simulations are compared for the four



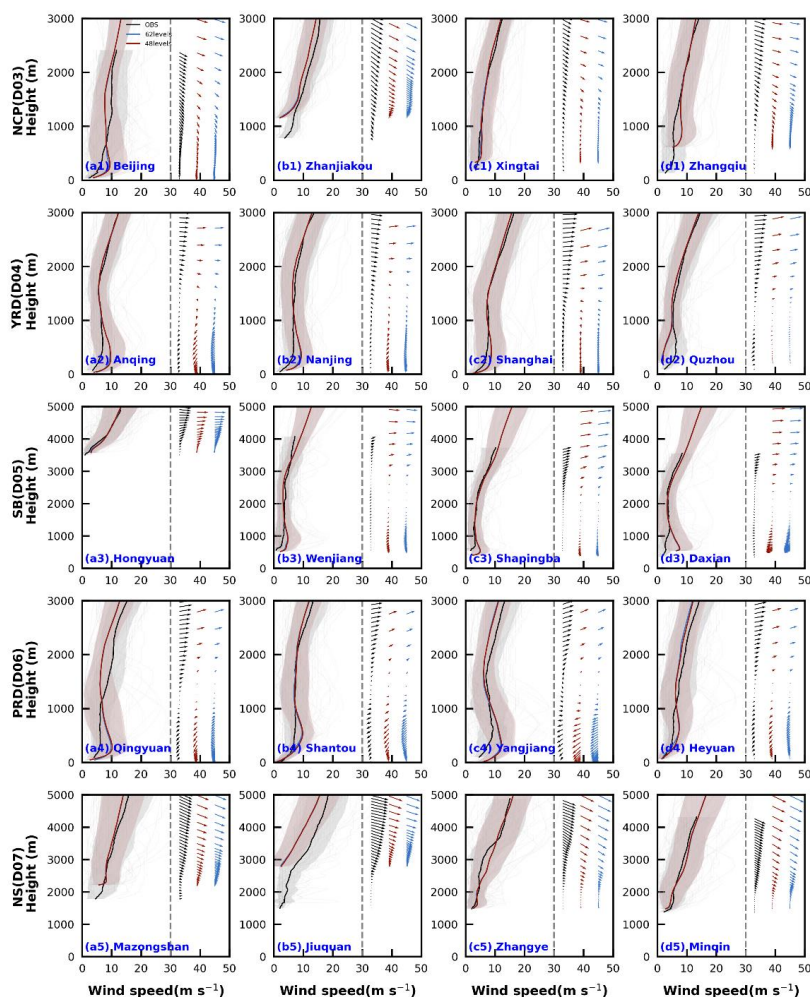
248 sounding stations selected for each region in Part I. As can be seen from Figure 6, the re-encryption
249 of the vertical resolution has no effect on the simulation of the temperature, regardless of the region.
250 The simulation results of the two experiments almost overlap in the vertical direction, implying that
251 the vertical structure of 48 levels is sufficient. On the contrary, the encryption of vertical resolution
252 affects the simulation results of wind speed to a certain extent, but the effect is marginal, especially
253 for high altitude regions like SB and NS (Fig. 7). For the YRD and PRD regions, the wind speed
254 simulated in Exp4 is less than that of Exp3 below 1000 m, with a difference of less than 1 m s^{-1} .
255 However, the encryption of the vertical resolution causes an increase in memory, which would add
256 about 5 GB of memory for a region of 1-day results, and the 150 GB for a month. Therefore, the
257 improvement in wind speed in some areas, due to the increase in vertical resolution, is not worth
258 the cost of increased memory, as the improvement is simply too insignificant.



259
260 **Figure 5. Vertical levels distribution for the two experiments of σ below 2 km in the model.**



261
262 **Figure 6.** Average vertical profiles of observed and simulated temperature at 08:00 and 20:00 BJT
263 at four sounding stations for each region in January. The unobtrusive gray lines indicate the
264 simulated lines for all time periods, and the lines with shading indicate the average values and
265 shaded areas show the uncertainty range (the mean ± 1 standard deviation).



266

267

Figure 7. Similar as Figure 6, but for 10-m wind speed and direction.

268

It is not necessary to set the vertical resolution much finer compared to the horizontal resolution,

269

and in this experiment, 48 levels are fully sufficient to reproduce the vertical structure of the PBL.

270

3.3 near-surface (N-S) scheme impact on PBL structures

271

For the impact of the N-S scheme, this section focuses on the changes in the N-S meteorological

272

parameters.

273

The N-S and PBL schemes are fixed pairings, and three experiments (i.e., Exp5, Exp6 and Exp7)

274

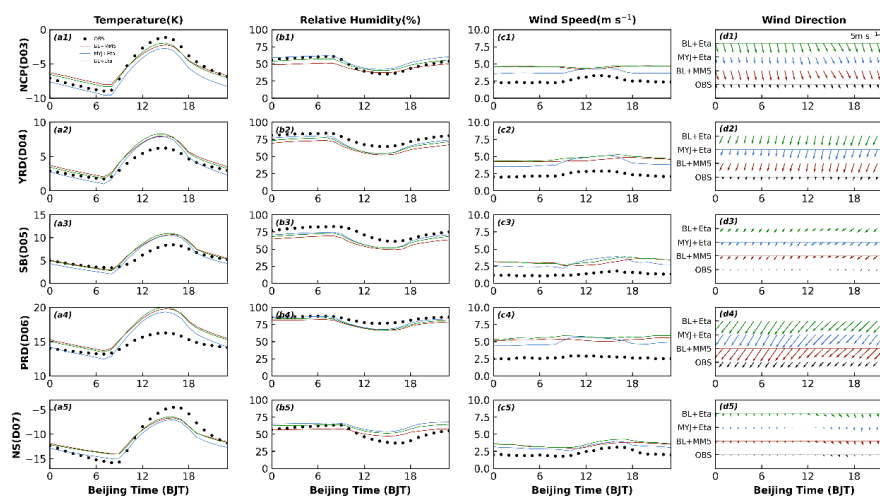
are done by this study to distinguish the extent to which the N-S and PBL schemes affect the N-S

275

meteorological parameters (2-m temperature, 2-m relative humidity, 10-m wind speed and direction).



276 In terms of daily variation, the variation of temperature in the five regions is consistent, with similar
277 simulated results in Exp5 (BL+MM5) and Exp7 (BL+Eta), and two experiments have notable
278 differences from Exp6 (MYJ+Eta) (Fig. 8a1-a5). However, the relative humidity and temperature
279 are different, and the results of Exp5 and Exp7 are not close to each other (Fig. 8b1-b5). From the
280 results of wind speed, it is similar to the results of temperature, and the results of Exp5 and Exp7
281 are much closer, as is the wind direction (Fig. 8c1-d5). Furthermore, the three schemes are made
282 differential to quantify the impact of the PBL scheme and N-S scheme. Exp6-Exp7 note the impact
283 of the PBL scheme, and Exp5-Exp7 illustrate the effect of the N-S scheme.

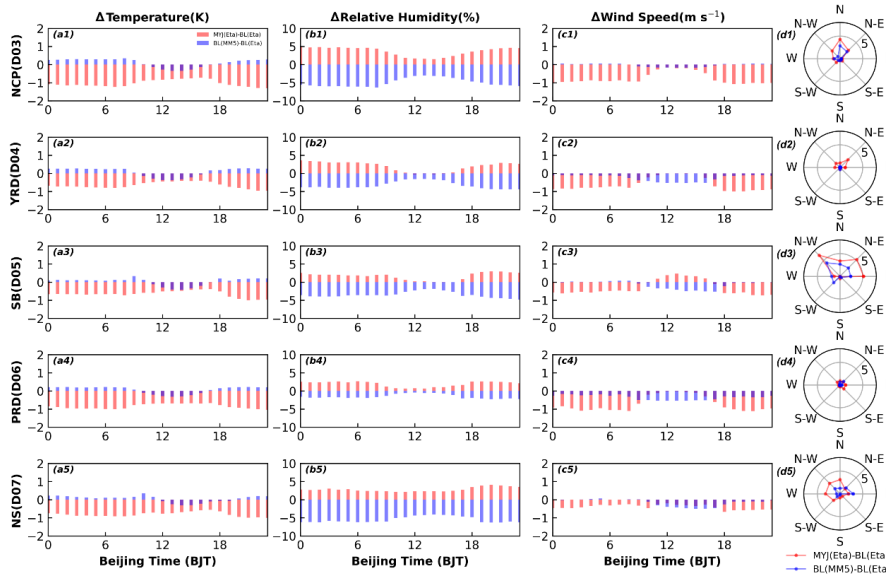


284
285 **Figure 8.** Time series of diurnal variation of (a1-a5) 2-m temperature, (b1-b5) 2-m relative
286 humidity, (c1-c5) 10-m wind speed and (d1-d5) 10-m wind direction for five regions in January.

287 As can be seen from Fig. 9a1-a5, the influence of the PBL scheme is greater compared to the N-S
288 scheme in five regions. The difference in temperature simulated by different PBL schemes is about
289 1 K, while the difference for N-S schemes is just less than 0.5 K. In Figure 9b1-b5, as in Figure 8,
290 the results for relative humidity differ from those for temperature. The PBL scheme does not affect
291 the relative humidity to the same extent as the N-S scheme, and it is also less than the N-S scheme.
292 Particularly in the NCP, SB, and NS regions, the impact of the PBL scheme is much smaller than
293 that of the N-S scheme (Fig. 9b1, b3, b5). Regardless of the PBL scheme and N-S scheme, the effect
294 is greater at night than during the day. The findings for wind speed and temperature are more similar,
295 with the PBL scheme having a remarkably greater impact than the N-S scheme (Fig. 9c1-c5). Except
296 for the daytime in both YRD and PRD regions, the N-S scheme has a slightly greater effect on wind

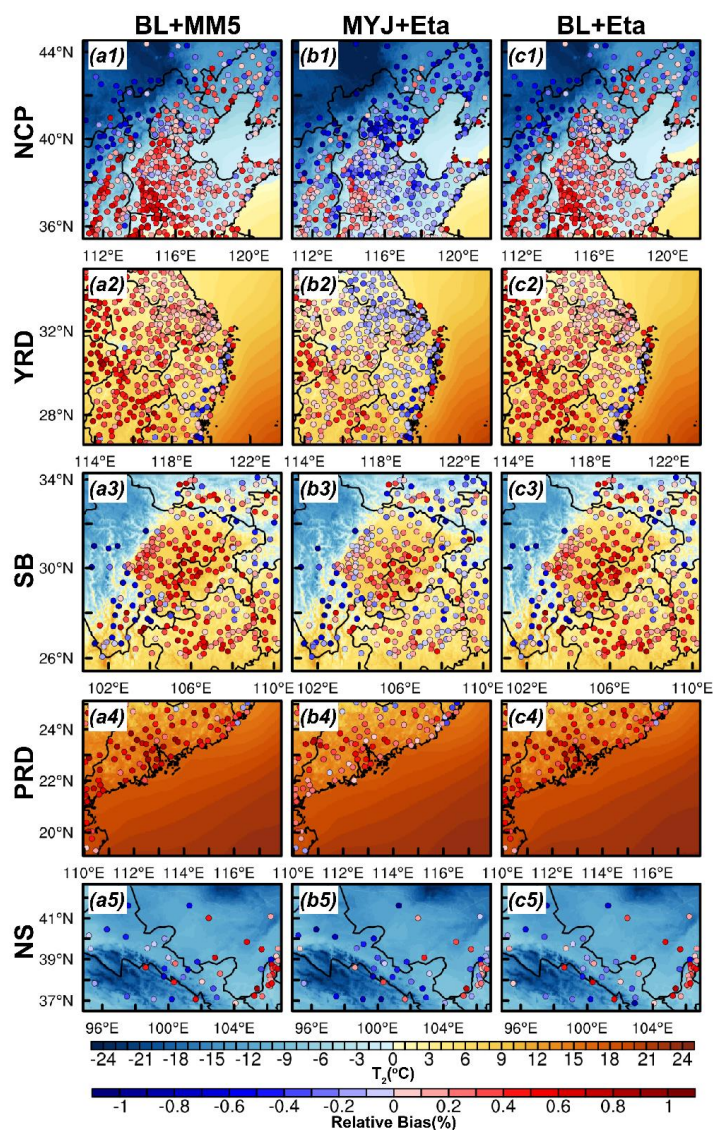


297 speed than the PBL scheme (Fig. 9c2, c4). The wind direction is divided into a total of eight
 298 directions (N, N-E, E, S-E, S, S-W, W, N-W), and the influence of the PBL scheme is larger as to
 299 the percentage frequency of each direction (Fig. 9 d1-d5).



300
 301 **Figure 9.** Time series of diurnal variation of the effects of PBL scheme and N-S scheme on (a1-a5)
 302 2-m temperature, (b1-b5) 2-m relative humidity, (c1-c5) 10-m wind speed and (d1-d5) 10-m wind
 303 direction for five regions in January.

304 As for the regional distribution of temperatures, the distribution of Exp5 and Exp7 is more similar,
 305 without regard to the region, and it differs considerably from that of Exp6 (Fig. 10). Therefore, for
 306 temperature, the effect of the PBL scheme is more important. For wind speed, Exp7 simulates the
 307 largest wind speed, followed by Exp5, and Exp6 has the smallest wind speed, noting that the PBL
 308 scheme has a larger degree of influence than the N-S scheme (Fig. 11).

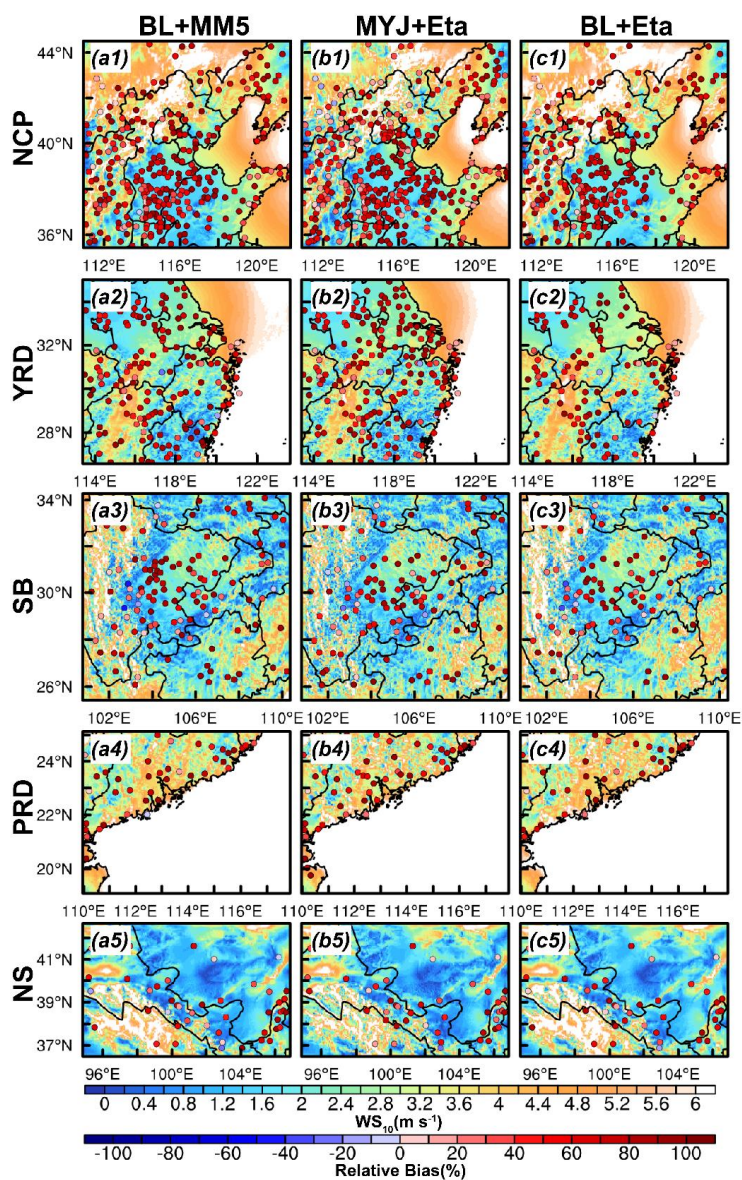


309
 310 **Figure 10. Regional distribution of 2-m temperature simulated by the (a) BL+MM5, (b) MYJ+Eta**
 311 **and (c) BL+Eta for five regions in January, and distribution of relative bias between simulations**
 312 **and observations is denoted by scatters.**

313 In general, for temperature, the choice of PBL scheme is of much more importance. For relative
 314 humidity, the PBL and N-S schemes are equally important, except for the NCP, SB and NS regions,
 315 where the choice of the N-S scheme is more principal. For wind speed and direction, the choice of
 316 PBL scheme is more critical, and the simulation of different PBL schemes leads to more differences



317 in the results.



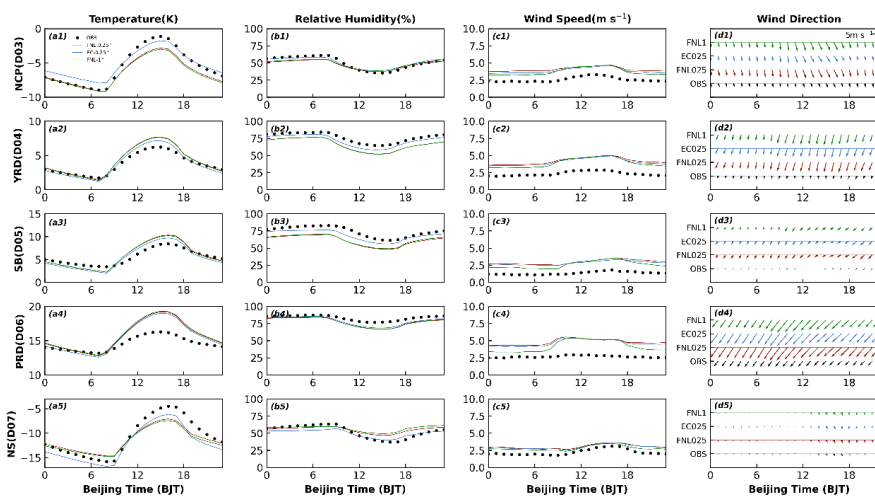
318
 319 **Figure 11.** Similar as Figure 10, but for 10-m wind speed.

320 **3.4 effect of initial and boundary conditions on meteorological parameters**

321 In this subsection, the same initial field and boundary conditions at different resolutions (i.e., FNL–
 322 1° and FNL–0.25°) and different initial field and boundary conditions at the same resolution (i.e.,



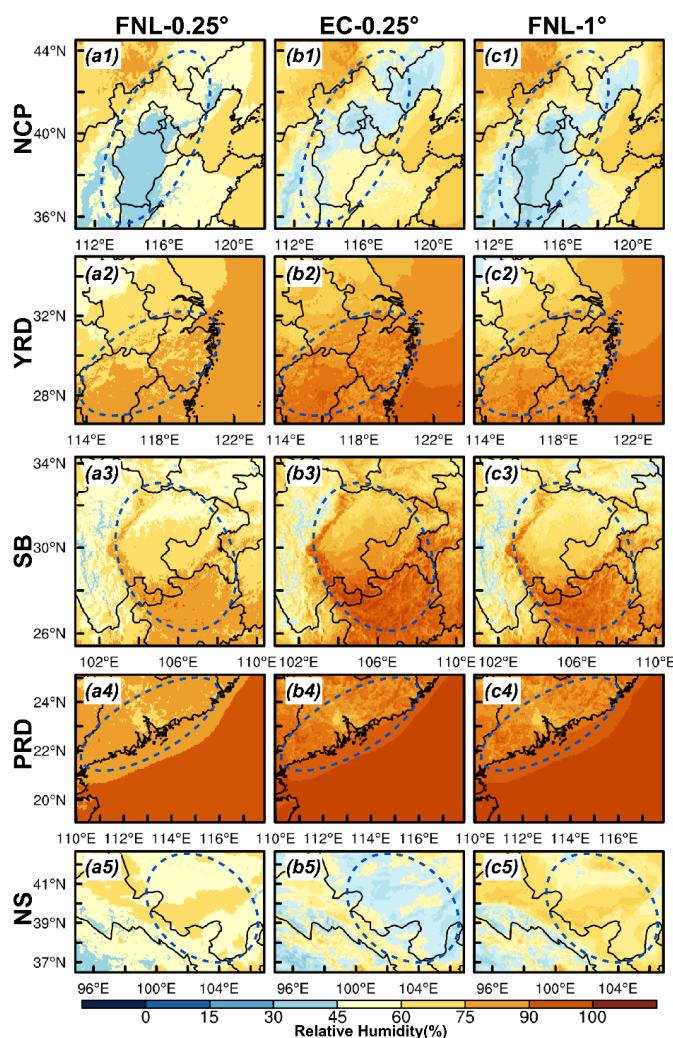
323 FNL-0.25° and EC-0.25°) are chosen to explore the effects of the initial field and boundary
324 conditions on the meteorological field simulation. Figure 12 shows the daily variation series of 2-m
325 temperature, 2-m relative humidity and 10-m wind speed and direction. Also, Figure 12 notes that
326 for temperature and relative humidity, the effect of data with different resolutions of the same initial
327 field on the results is small, but the effect of data with different initial fields of the same resolution
328 is profound. For the five regions, the EC data better simulate the temperature than the FNL data
329 during the day, while at night, the difference between the two types of data simulating the
330 temperature becomes less than during the day, except for the NCP and NS regions (where the
331 temperature difference is larger for both day and night) (Fig. 12 a1-a5). For relative humidity, the
332 EC data are simulated better than the FNL data regardless of the region, playing a key role in
333 improving the relative humidity results of the model (Fig. 12 b1-b5). Overall, the increase in
334 resolution of the initial field data from 1° to 0.25° has less effect on the simulation of temperature
335 and relative humidity, while there is a striking difference between the different initial field data.



336
337 **Figure 12. Similar as Figure 8, but for different initial and boundary conditions.**
338 The results for wind speed differ from the first two parameters in that there is almost no difference
339 between the three experiments for wind speed simulations during the day (Fig. 12 c1-c5). However,
340 different initial field data at the same resolution have very little effect on the wind speed, but the
341 same initial field data at different resolutions have a significant effect on the wind speed, especially
342 at night (Fig. 12c1-c5). All data have a negligible effect on the wind direction (Fig. 12 d1-d5).
343 The EC data have improved the results of relative humidity for all regions as mentioned earlier (Fig.



344 12 b1-b5). In terms of regional distribution, the regional distribution of FNL data is similar in shape
345 for different resolutions (Fig. 13 a, c). However, the relative humidity distribution simulated by EC
346 data and FNL data is drastically different (Fig. 13). It is worth noting that the relative humidity of
347 the EC data is the highest in the four regions except for the NS region in which the relative humidity
348 is the lowest (Fig. 13 b1-b5).



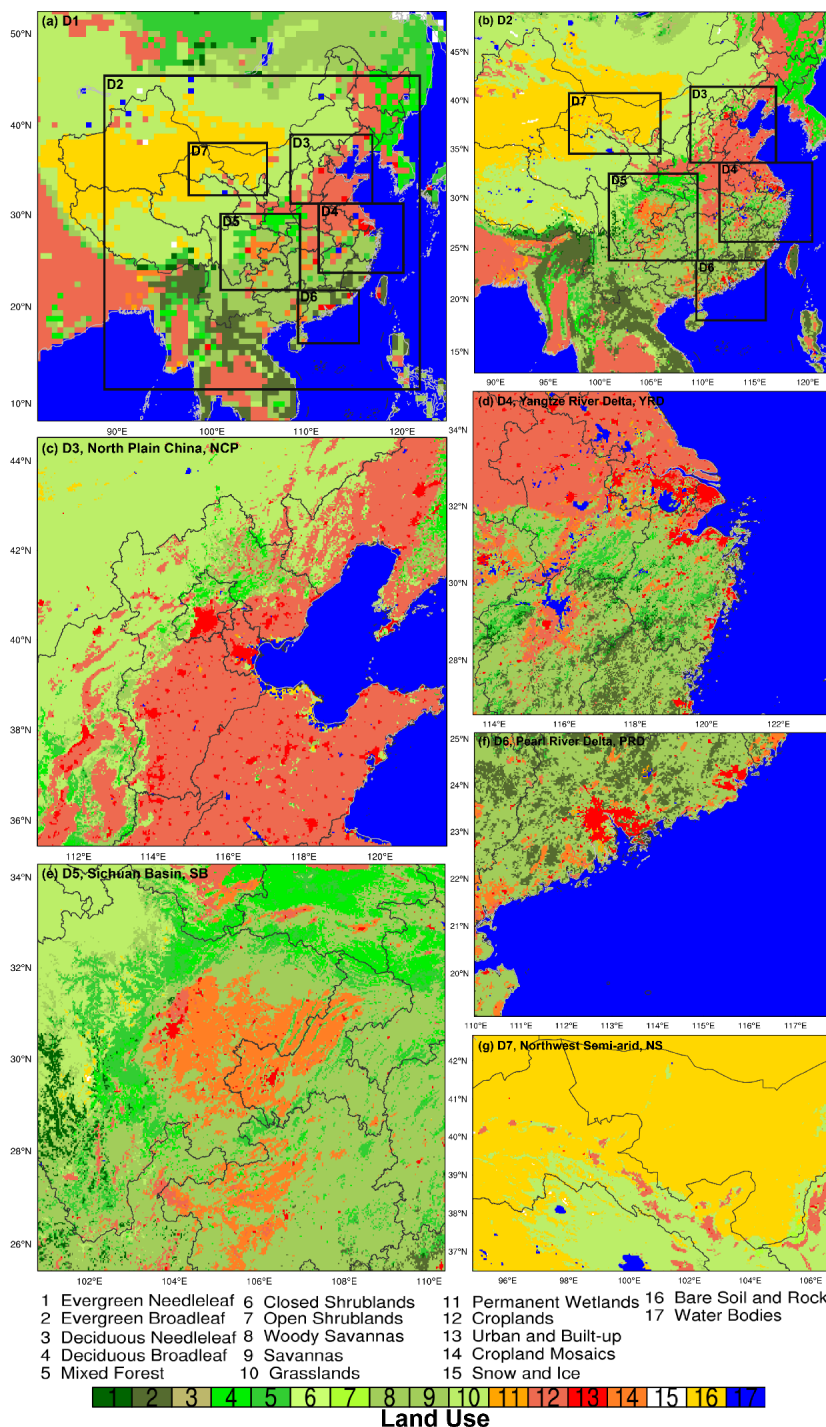
349
350 **Figure 13.** Regional distribution of 2-m relative humidity simulated by the (a) FNL-0.25°, (b) EC-
351 0.25° and (c) FNL-1° for five regions in January, and the blue dashed circles indicate the regions
352 where the results of the three experimental simulations differ significantly.
353 In the vertical direction, the simulated results of the three experiments for temperature and wind



354 speed do not differ much, unlike the near-surface meteorological parameters (i.e., T2, RH2, WS10
355 and WD10) that show such obvious differences (Fig. S1, S2). Nevertheless, for the relative humidity,
356 the variation in vertical direction at different heights is more consistent with the near-surface layer,
357 where the relative humidity of EC data is high in the whole layer (Fig. S3). Except for a few highland
358 stations outside the basin in the SB region, the relative humidity of EC data is low at higher altitudes
359 (Fig. S3 a3, b3, d3).

360 3.5 effect of underlying surface on meteorological parameters

361 To further explore the impact of underlying surface changes on the simulation results of
362 meteorological fields, we use the underlying surface data in January 2016 that is closer to the
363 simulation time, in addition to the default underlying surface data that comes with the model, for
364 comparative analysis of the simulation. Comparing Figure 1 and Figure 14, it can be concluded that
365 the most substantial change in the Domain 1 area is in the croplands type (i.e., code 12), especially
366 for the area south of latitude 30 °N. Many types with an underlying surface of 12 have become 14
367 or 8, 9 etc. Although both 12 and 14 here can represent cropland, there are some differences in the
368 specific descriptions. Code 12 mainly indicates that at least 60% of area is cultivated cropland, while
369 code 14 mainly refers to the mosaics of small-scale cultivation 40–60% with natural tree, shrub, or
370 herbaceous vegetation. In addition to croplands, the two types of urban and water bodies are more
371 variable as well. Therefore, this subsection focuses on the effects of urban and water body changes
372 on surface meteorological fields.



373

374

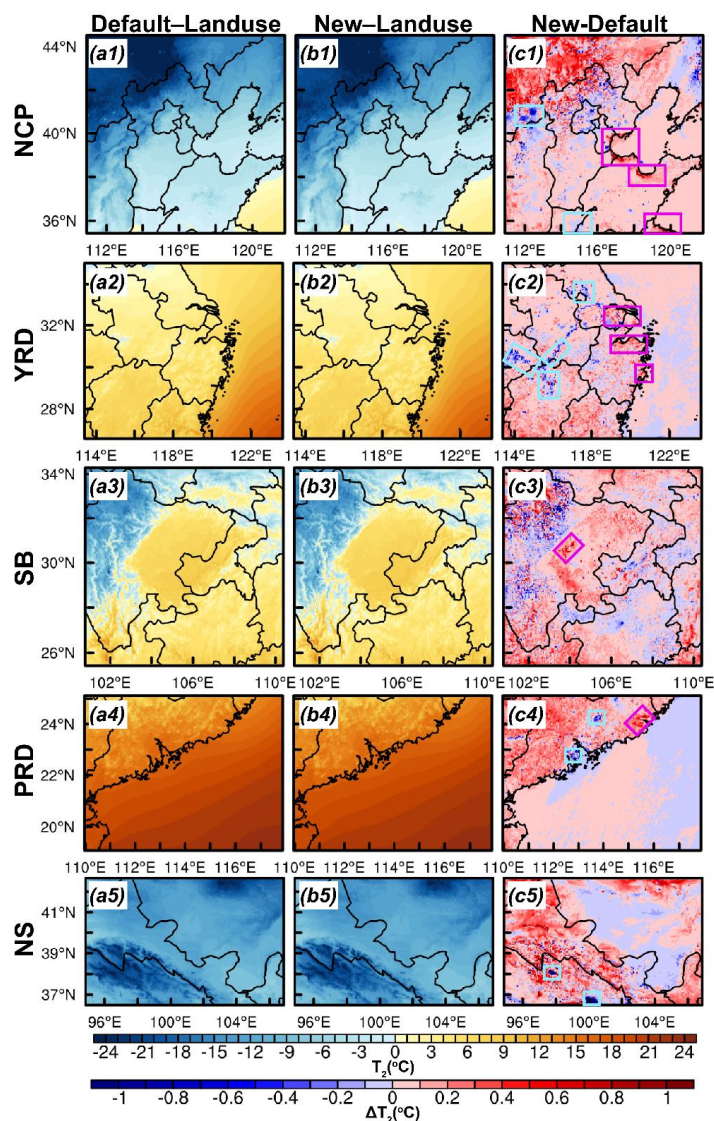
Figure 14. Similar as Figure 1, but for the land use type for January 2016.



375

376 In terms of the overall regional distribution, the new underlying surface did not affect the areas of
377 high and low values of temperature (Fig. 15 a-b) to an important degree. However, the difference
378 between the simulation results of two different underlying surface shows that the change of the
379 underlying surface has an effect on the temperature by about ± 1 °C, especially for the grids with
380 more obvious changes in water bodies and urban areas (Fig. 15 c). In the NCP region, an increase
381 in the area of water bodies in the coastal areas of Tianjin, Shandong Peninsula, and Jiangsu Province
382 leads to a distinct increase in temperature (i.e., indicated by red boxes), while a decrease in the area
383 of inland water in the northern region of Shanxi Province causes a decrease in temperature (i.e.,
384 denoted by blue boxes) (Fig. 15 c1). The decrease in the area of water bodies in the Yangtze River
385 in the YRD region has caused a decrease in temperature, while urbanization has contributed to an
386 increase in temperature in several regions (Fig. 15 c2). The underlying surface changes in the SB
387 region are mainly in the form of forest and savannas changes, as well as the more rapid urbanization
388 of the provincial capital city of Chengdu (Fig. 14 e). The development of this city has a positive
389 feedback effect on the temperature of the region (Fig. 15 c3). The underlying surface change in the
390 YRD region is from croplands to savannas, with a rapid greening rate, and its excessive greening
391 may make the green coverage of some cities too high, leading some grids to identify the cities as
392 savannas. In the NS region, the area of croplands and cities along the Qilian Mountains increases
393 and the area of some inland lakes decreases, in turn leaving some influence on the results of the
394 temperature.

395 The wind field does not vary as regularly as the temperature field. Except for the variation of water
396 body area which has a more consistent pattern on the wind field, all other types of underlying surface
397 variation have a haphazard effect on the wind field (Fig. S4).



398

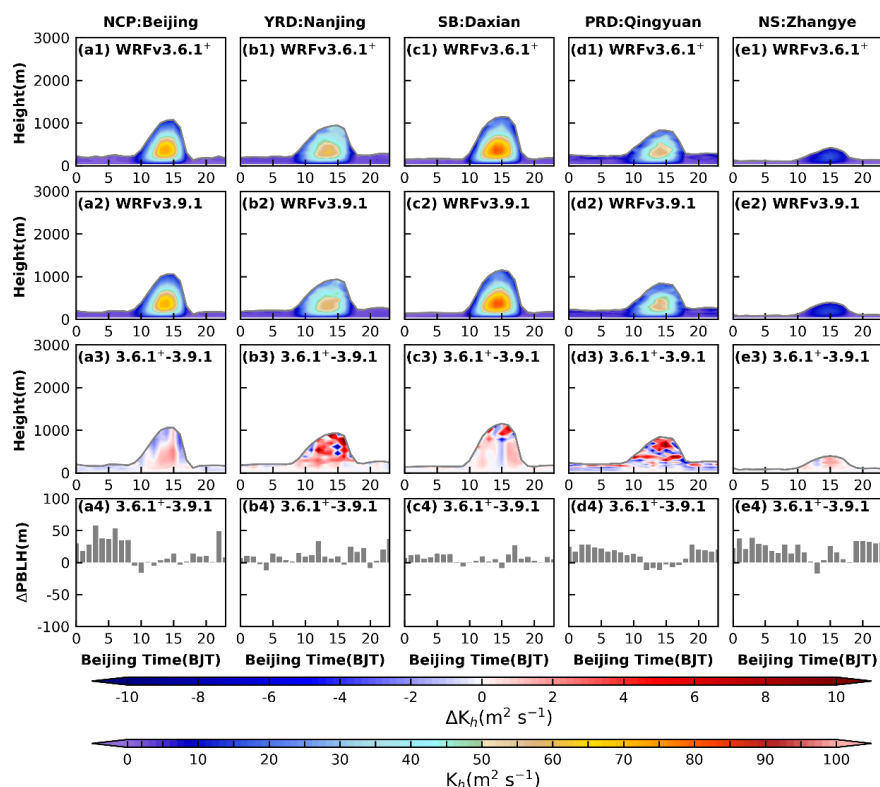
399 **Figure 15. Regional distribution of 2-m temperature simulated by the (a) default land use, (b) new**
 400 **land use and (c) the difference between the two land use types for five regions in January. The blue**
 401 **(red) box indicates the region where the wind speed decreases (increases) due to changes in the**
 402 **water bodies and urban.**

403 **3.6 impact of the model version update**

404 **As computer technology continues to evolve, the parameterizations in the model are being upgraded**



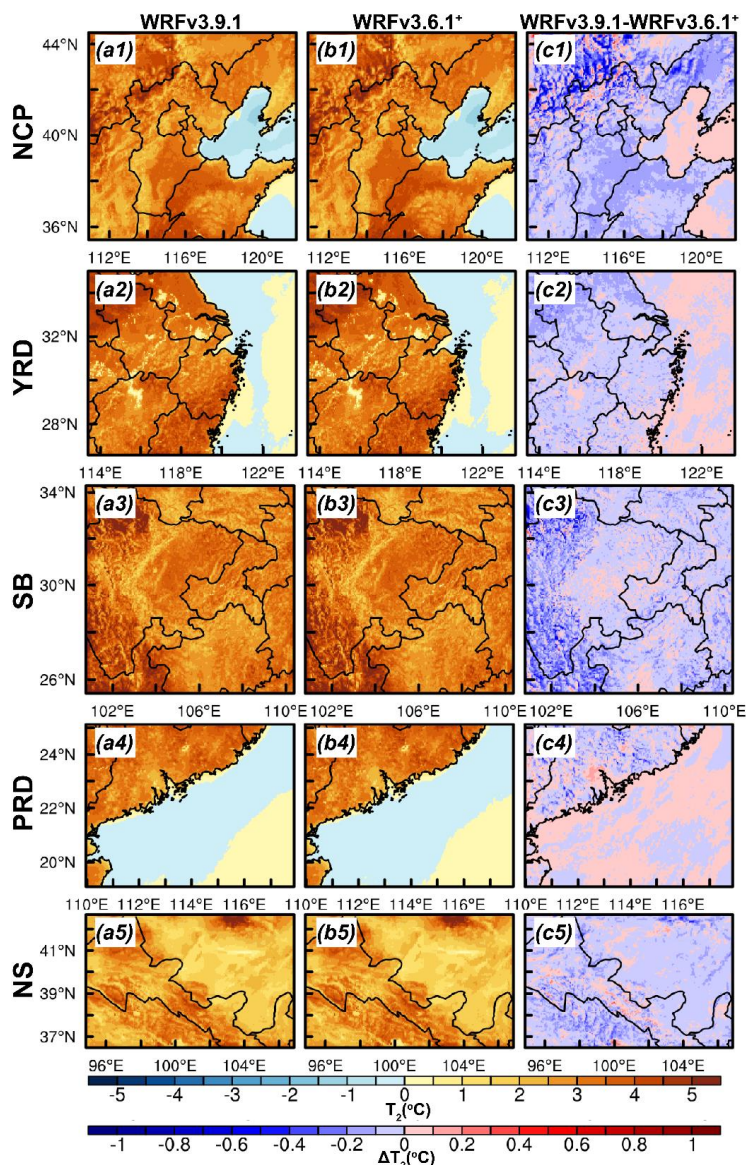
405 and improved, but it is worthwhile further exploring how much the parameterizations and versions
 406 affect the simulation results of the model. For the PBL parameterization scheme, turbulent diffusion
 407 is crucial for the vertical mixing of momentum, heat, water vapor and pollutants within the PBL.
 408 And in December 2014, the ACM2 parameterization scheme received two major updates: (1) The
 409 turbulent diffusion coefficients of heat are updated. The stability function of Richardson number is
 410 modified, expecting to reduce the day and night 2-m temperature bias. (2) The bug that the minimum
 411 value of the PBLH is lower than the height of the first level of the model under stable conditions
 412 has been restored, and the minimum value of the PBLH is fixed to the height of the first level of the
 413 model. We, therefore, choose the ACM2 scheme in WRFv3.6.1 as a control experiment. In the
 414 control experiment, the ACM2 scheme in the WRFv3.9.1 version is replaced with WRFv3.6.1, and
 415 all other schemes are kept in the WRFv3.9.1 (i.e., WRFv3.6.1⁺). This ensures that the difference
 416 between the two experiments is the representative of the impact of the ACM2 scheme update.



417
 418 Figure 16. Time-height cross sections of heat turbulent diffusion coefficient (TDC) simulated by
 419 (a1-e1) WRFv3.6.1⁺, (a2-e2) WRFv3.9.1, (a3-e3) the difference between the TDC of the two versions.



- 420 (a4-e4) Time series of diurnal variation of the difference between the PBLH of the two versions.
 421 The gray line in (a1-e3) indicates the PBLH.



- 422
 423 **Figure 17.** Similar as Figure 15, but for the effects of model versions.
 424 The difference between the turbulent diffusion coefficient of heat calculated by the two versions lies
 425 in the different principles of calculation using the Richardson number (Ri) method. In the
 426 WRFv3.6.1+, not only Ri is used to judge the stability, but also z/L is used to additionally constrain



427 the stability and determine the empirical stability function. In contrast, only Ri is adopted to
428 determine the function in the WRFv3.9.1. Figure 16 shows the diurnal variation of turbulent
429 diffusion coefficient of heat with height, as well as the difference of PBLH. In general, the two
430 versions have no effect on the overall trend of TDC (Fig. 16 a1-e2). However, within the PBL, the
431 TDC of WRFv3.9.1 is smaller than that of WRFv3.6.1+, with the most significant difference during
432 the daytime. Meanwhile, in some regions at night, a TDC of WRFv3.9.1 is also greater than that of
433 WRFv3.6.1+ (Fig. 16 a3-e3). Besides, the differences among the five regions slightly vary. The
434 deviation in the NCP, SB, and NS regions is small, around $2 \text{ m}^2 \text{ s}^{-1}$ (Fig. 16 a3, c3, e3), while the
435 deviation in the YRD and PRD regions is large, up to about $10 \text{ m}^2 \text{ s}^{-1}$ (Fig. 16 b3, d3). The TDC
436 modification aims to reduce the temperature difference between day and night. Indeed, this
437 expectation is fulfilled. It can be noticed in Figure 17, the diurnal temperature difference for
438 WRFv3.9.1 is smaller than that of WRFv3.6.1+ in almost all regions (except for the area where the
439 underlying surface is water). In addition, we need to pay attention to the variation of the PBLH. As
440 shown in Figure 16, the difference in PBLH during daytime is smaller than at night, and the PBLH
441 of WRFv3.9.1 is lower than that of WRFv3.6.1+. The model WRFv3.9.1 fixes the minimum value
442 of the PBLH to the first level height, markedly reducing the PBLH at night. But this approach may
443 be too crude and parsimonious to cause problems, and should be corrected in the future.

444 4 Conclusion

445 The simulation results of the model within the PBL are subject to many factors, but its portrayal and
446 description by the PBL parameterization schemes plays a vital role in affecting the variation of the
447 meteorological field. The simulations of the PBL schemes on the meteorological fields has been
448 described in Part I. In Part II, further uncertainties affecting the results of the meteorological field
449 are evaluated and analyzed, and the degree of influence of different factors is compared, hoping to
450 provide a reference for scholars conducting research on the model.

451 In addition to the dominant role of the PBL scheme on the results of the meteorological field, many
452 elements in the model are influenced by large uncertainties. For example, what is the effect of
453 horizontal resolution, and how much does the result vary under different resolution conditions? Is
454 the continuous encryption of the vertical levels necessary for the simulation of the vertical structure
455 of the PBL? Which has a greater impact on the results of the meteorological field, the near-surface
456 (N-S) layer scheme or the PBL scheme? How much is the impact of these changes on the underlying



457 surface, which is constantly updated by the development of urbanization? The innovation of
458 computer technology has brought the opportunity to keep the model being updated. How much
459 effect will the updates have on different versions of the model results? The simulation of the model
460 depends on the initial and boundary conditions, so how much does the initial and boundary
461 conditions of different resolutions and products affect the model results? These uncertainties have
462 not been fully evaluated and analyzed yet. To resolve the confusions, this study synthesizes the
463 effects of the above factors on the model results.

464 *a. Effect of the horizontal resolution.* The three different resolutions have a more dramatic effect
465 on temperature than on wind speed. Regardless of the region, the distribution of temperature
466 deviations simulated at 75 km resolution is clearly different from that of 15 km and 3 km,
467 especially in areas with more complex topography, such as NCP, SB and NS regions. All three
468 resolutions overestimate the wind speed in all regions, except for the 75 km resolution, where
469 there is an underestimation of the wind speed at the stations around the basin in the SB region.
470 The difference between the resolutions decreases with increasing temperature, but becomes
471 more pronounced with increasing wind speed.

472 *b. Effect of the vertical resolution.* The number of vertical levels of the model is encrypted from
473 48 to 62 levels, with almost no effect on the vertical structure of the PBL. Meanwhile, the
474 increase in the number of vertical levels brings into an increase in memory of about 150 GB for
475 one month. Compared to the horizontal resolution, the vertical resolution does not need to be
476 set particularly fine, and 48 levels are perfectly sufficient to reproduce the evolution of the PBL
477 structure.

478 *c. Influence of the N-S scheme.* The PBL scheme makes a greater impact on the simulated results
479 for temperature, wind speed and direction, while for relative humidity, the N-S scheme
480 contributes largely, especially in the NCP, SB and NS regions. For either scheme, the effect is
481 much greater at night than during the daytime. In general, the choice of the PBL scheme is more
482 critical for temperature and wind fields. But for relative humidity, the PBL and N-S schemes
483 are equally important.

484 *d. Impact of the initial and boundary conditions.* The effect of data of different resolutions of the
485 same product on the results of temperature and relative humidity is small, but the influence of
486 data of different products of the same resolution is large. EC data simulates temperature better
487 than FNL data during the daytime, while at night, the difference between the two data is



488 relatively small (except for the NCP and NS regions). The EC data simulate the relative
489 humidity better than the FNL data regardless of the region, even in the vertical direction, which
490 will exposes a key way to improve the relative humidity results of the model in the future.
491 Nonetheless, data of the same resolution but different products exhibit no obvious effect on
492 wind speed, while the influence of data from the same product with different resolutions is
493 larger, especially at night.

494 *e. Effect of the underlying surface.* In terms of regional distribution, the new underlying surface
495 make no significant difference with respect to the temperature. However, for the grids with
496 more pronounced changes in water bodies and urban, the change in underlying surface has an
497 approximate $\pm 1^\circ\text{C}$ influence on temperature. An increase (decrease) in the area of water bodies
498 leads to an increase (decrease) in temperature, and the growth of urbanization brings about an
499 increase in temperature. The variation of wind field is not as regular as temperature. Except for
500 the changes in the area of water bodies that affect the wind filed consistently, other types of
501 underlying surface changes show a haphazard effect on the wind filed.

502 *f. Influence of the model version.* The update of the PBL scheme reduces the day and night 2-m
503 temperature bias. But the simple definition method of fixing the minimum value of the PBLH
504 as the first level height of the model may have some defects. The change in the stability function
505 of the Richardson number alters the turbulent diffusion coefficient of heat, which is more
506 distinct in the daytime with a deviation of about $10\text{ m}^2\text{ s}^{-1}$.

507 In summary, the horizontal resolution is more influential than the vertical resolution. The N-S
508 scheme has less effect than the PBL scheme on the results of temperature and wind speed. Also,
509 the initial and boundary conditions of different products have the most significant influence on
510 relative humidity. Grid changes where the underlying surface is urban and water bodies have a
511 more pronounced effect on the results of meteorological fields, especially for temperature. The
512 constant updating of the model version does not necessarily optimize the simulation results
513 continuously. A special advice here is that the needs of different scholars for the model vary a
514 lot, thus, the configuration of uncertainties requires a comprehensive consideration to obtain
515 the optimal results for the analysis.

516 **Code and data availability**

517 The source codes of WRF version 3.9.1 and 3.6.1 can be found on the following website:
518 <https://www2.mmm.ucar.edu/wrf/users/download/>. The original model settings file is already



519 included in Supplement in Part I, while the other model settings file used in Part II is named after
520 the file name “L62_namelist.input” and is already included in Supplement. In addition, the
521 observations used are also provided in Supplement in Part I. The initial field and boundary condition
522 data and the underlying surface data are provided in the text.

523 Author contributions

524 Development of the ideas and concepts behind this work was performed by all the authors. Model
525 execution, data analysis and paper preparation were performed by WJ. XZ and HW provide
526 computing resources, and offer advice and feedback. YW, DW, and JZ support the data. WZ, LZ,
527 LG, YL, JW, YY, and YL provides suggestions. All authors contributed to the manuscript.

528 Competing interests

529 The authors declare that they have no conflict of interest.

530 Acknowledgements.

531 The work was carried out at the National Supercomputer Center in Tianjin, and the calculations
532 were performed on TianHe-1 (A).

533 Financial support

534 This research is supported by NSFC Major Project (42090031), NSFC Project (U19A2044).

535

536 References

- 537** Bhati, S., and Mohan, M. WRF model evaluation for the urban heat island assessment under varying
538 land use/land cover and reference site conditions. *Theoretical and Applied Climatology*,
539 *126*(1), 385–400. doi:10.1007/s00704-015-1589-5, 2016.
- 540** Chang, P., Zhang, S., Danabasoglu, G., Yeager, S. G., Fu, H., Wang, H., et al. An Unprecedented Set
541 of High-Resolution Earth System Simulations for Understanding Multiscale Interactions in
542 Climate Variability and Change. *Journal of Advances in Modeling Earth Systems*, *12*(12),
543 e2020MS002298. doi:10.1029/2020MS002298, 2020.
- 544** Friedl, M. A., McIver, D. K., Hodges, J. C. F., Zhang, X. Y., Muchoney, D., Strahler, A. H., et al.
545 Global land cover mapping from MODIS: algorithms and early results. *Remote Sensing of*
546 *Environment*, *83*(1), 287–302. doi:10.1016/S0034-4257(02)00078-0, 2002.



- 547** García-García, A., Cuesta-Valero, F. J., Beltrami, H., González-Rouco, J. F., and García-Bustamante,
548 E. WRF v3.9 sensitivity to land surface model and horizontal resolution changes over
549 North America. *Geosci. Model Dev.*, *15*(2), 413-428. doi:10.5194/gmd-15-413-2022, 2022.
- 550** Li, D., Chang, P., Yeager, S. G., Danabasoglu, G., Castruccio, F. S., Small, J., et al. The Impact of
551 Horizontal Resolution on Projected Sea-Level Rise Along US East Continental Shelf With
552 the Community Earth System Model. *J Adv Model Earth Syst*, *14*(5), e2021MS002868.
553 doi:10.1029/2021MS002868, 2022.
- 554** Li, J., Bao, Q., Liu, Y., Wang, L., Yang, J., Wu, G., et al. Effect of horizontal resolution on the
555 simulation of tropical cyclones in the Chinese Academy of Sciences FGOALS-f3 climate
556 system model. *Geosci. Model Dev.*, *14*(10), 6113-6133. doi:10.5194/gmd-14-6113-2021,
557 2021.
- 558** Li, Y., Gao, Z., Lenschow, D. H., and Chen, F. An Improved Approach for Parameterizing Surface-
559 Layer Turbulent Transfer Coefficients in Numerical Models. *Boundary-Layer Meteorology*,
560 *137*(1), 153-165. doi:10.1007/s10546-010-9523-y, 2010.
- 561** Ma, Z., Liu, Q., Zhao, C., Shen, X., Wang, Y., Jiang, J. H., et al. Application and Evaluation of an
562 Explicit Prognostic Cloud-Cover Scheme in GRAPES Global Forecast System. *Journal of*
563 *Advances in Modeling Earth Systems*, *10*(3), 652-667. doi:10.1002/2017MS001234, 2018.
- 564** Ma, Z., Zhao, C., Gong, J., Zhang, J., Li, Z., Sun, J., et al. Spin-up characteristics with three types
565 of initial fields and the restart effects on forecast accuracy in the GRAPES global forecast
566 system. *Geoscientific Model Development*, *14*(1), 205-221. doi:10.5194/gmd-14-205-2021,
567 2021.
- 568** Magnusson, L., and Källén, E. Factors Influencing Skill Improvements in the ECMWF Forecasting
569 System. *Monthly Weather Review*, *141*(9), 3142-3153. doi:10.1175/mwr-d-12-00318.1,
570 2013.
- 571** Menut, L., Bessagnet, B., Colette, A., and Khvorostiyarov, D. On the impact of the vertical
572 resolution on chemistry-transport modelling. *Atmospheric Environment*, *67*, 370-384.
573 doi:10.1016/j.atmosenv.2012.11.026, 2013.
- 574** Morichetti, M., Madronich, S., Passerini, G., Rizza, U., Mancinelli, E., Virgili, S., et al. Comparison
575 and evaluation of updates to WRF-Chem (v3.9) biogenic emissions using MEGAN. *Geosci.*
576 *Model Dev.*, *15*(16), 6311-6339. doi:10.5194/gmd-15-6311-2022, 2022.
- 577** Nolan, D. S., and Onderlinde, M. J. The Representation of Spiral Gravity Waves in a Mesoscale
578 Model With Increasing Horizontal and Vertical Resolution. *Journal of Advances in*
579 *Modeling Earth Systems*, *14*(8), e2022MS002989. doi:10.1029/2022MS002989, 2022.
- 580** O'Dea, E., Furner, R., Wakelin, S., Siddorn, J., While, J., Sykes, P., et al. The CO5 configuration of
581 the 7 km Atlantic Margin Model: large-scale biases and sensitivity to forcing, physics
582 options and vertical resolution. *Geosci. Model Dev.*, *10*(8), 2947-2969. doi:10.5194/gmd-



- 583 10-2947-2017, 2017.
- 584 Qian, Y., Chakraborty, T. C., Li, J., Li, D., He, C., Sarangi, C., et al. Urbanization Impact on Regional
585 Climate and Extreme Weather: Current Understanding, Uncertainties, and Future Research
586 Directions. *Adv Atmos Sci*, 39(6), 819-860. doi:10.1007/s00376-021-1371-9, 2022.
- 587 Roberts, M. J., Jackson, L. C., Roberts, C. D., Meccia, V., Docquier, D., Koenigk, T., et al.
588 Sensitivity of the Atlantic Meridional Overturning Circulation to Model Resolution in
589 CMIP6 HighResMIP Simulations and Implications for Future Changes. *Journal of*
590 *Advances in Modeling Earth Systems*, 12(8), e2019MS002014.
591 doi:10.1029/2019MS002014, 2020.
- 592 Rummukainen, M. Added value in regional climate modeling. *WIREs Climate Change*, 7(1), 145-
593 159. doi:10.1002/wcc.378, 2016.
- 594 Singh, J., Singh, N., Ojha, N., Sharma, A., Pozzer, A., Kiran Kumar, N., et al. Effects of spatial
595 resolution on WRF v3.8.1 simulated meteorology over the central Himalaya. *Geosci. Model*
596 *Dev.*, 14(3), 1427-1443. doi:10.5194/gmd-14-1427-2021, 2021.
- 597 Small, R. J., Bacmeister, J., Bailey, D., Baker, A., Bishop, S., Bryan, F., et al. A new synoptic scale
598 resolving global climate simulation using the Community Earth System Model. *Journal of*
599 *Advances in Modeling Earth Systems*, 6(4), 1065-1094. doi:10.1002/2014MS000363, 2014.
- 600 Taylor, K. E., Stouffer, R. J., and Meehl, G. A. An Overview of CMIP5 and the Experiment Design.
601 *Bulletin of the American Meteorological Society*, 93(4), 485-498. doi:10.1175/bams-d-11-
602 00094.1, 2012.
- 603 Teixeira, J. C., Carvalho, A. C., Tuccella, P., Curci, G., and Rocha, A. WRF-chem sensitivity to
604 vertical resolution during a saharan dust event. *Physics and Chemistry of the Earth, Parts*
605 *A/B/C*, 94, 188-195. doi:10.1016/j.pce.2015.04.002, 2016.
- 606 Tolentino, J., Rejuso, M. V., Inocencio, L. C., Ang, M. R. C., and Bagtasa, G. (2016). *Effect of*
607 *horizontal and vertical resolution for wind resource assessment in Metro Manila,*
608 *Philippines using Weather Research and Forecasting (WRF) model* (Vol. 10005): SPIE.
- 609 Weigel, A. P., Chow, F. K., and Rotach, M. W. The effect of mountainous topography on moisture
610 exchange between the “surface” and the free atmosphere. *Boundary-Layer Meteorology*,
611 125(2), 227-244. doi:10.1007/s10546-006-9120-2, 2007.
- 612 Zhou, B., Zhu, K., and Xue, M. A Physically Based Horizontal Subgrid-Scale Turbulent Mixing
613 Parameterization for the Convective Boundary Layer. *Journal of the Atmospheric Sciences*,
614 74(8), 2657-2674. doi:10.1175/jas-d-16-0324.1, 2017.
- 615